ADVANCED MATERIALS TECHNOLOGIES
www.advmattechnol.de

Measurement of Parachute Canopy Textile Deformation Using Mechanically Invisible Stretchable Lightguides

*Jeyeon Jo, Artemis Xu, Anand Kumar Mishra, Hedan Bai, Armen Derkevorkian, Jason Rabinovitch, Huiju Park, and Robert F. Shepherd**

Conventional strain gauges are not designed for accurate measurement over the large range of deformations possible in compliant textiles. The thin, lightweight, and flexible nature of textiles also makes it challenging to attach strain gauges in a way that does not affect the mechanical properties. In this manuscript, soft, highly extensible fibers that propagate light (i.e., stretchable lightguides) are stitched as a strain gauge to map the deformation of a nylon parachute textile under tension. When under load, these fiber optic strain gauges propagate less light, and this strain-induced light modulation is used to accurately (absolute error≈2.93%; Std. Dev.: 3.02%) measure strain in the <30% range before these textiles fail. This system has directionality; strain in parallel to the sensor results in little light attenuation while perpendicular loading shows high sensitivity (Gauge factor$_{\perp}$≈24.8 and Gauge factor$_{\parallel}$≈0.05 at the first 1% strain). Structural and optical simulations are coupled to demonstrate that load transfer on the fiber optic by the stitchwork is the dominating cause of signal modulation. To further validate the hypotheses, digital image correlation was used under dynamic loading conditions to show that these sensors do not significantly affect the mechanical properties.

1. Introduction

Textiles represent an important class of materials that consist of fibers with specific arrangements achieved by weaving, knitting, or felting. These textiles have a wide range of mechanical properties based on the complexity of the structure. For example, aramid fibers have elastic moduli ≈ 62 GPa < E < 190 GPa and ultimate strains 1% < γ_{ult}^{fiber} < 4.4%,[1,2] but can be extended much more ($\gamma_{ult}^{yarn} \approx 27\%$) in the form of yarn; knits from these yarns show 3–7 times higher ultimate strains (75% < $\gamma_{ult}^{textile}$ < 200%).[3] Textiles made of elastic fiber such as polyurethane (0.01 GPa < E < 0.03 GPa and γ_{ult}^{fiber} > 500%) can experience much larger deformation under a small amount of tension.[1] Products composed of textiles (e.g., clothing, architectural membranes, airbags, tube/inflatable boats, and parachutes) are typically used in complex loading conditions that are difficult to model, particularly due to the large range of mechanical properties.

Strain gauges can be placed surreptitiously onto textiles as a method to map deformation under these complex loading conditions.[4] Most commercially available strain gauges (e.g., Omega SGD-5) need to be well attached to or embedded into the substrate[5] and record changes in resistance or capacitance. They are often made of metal foils that are accurate to strains ≤5%,[6] so they are not compatible with the large strain ranges expected of textiles. Arranging the conductive material in a serpentine pattern can increase the strain range to ≈75%;[7] however, the high modulus of the foil affects the local deformation where adhesion takes place.[6] Thus, there is a need for strain gauges that can reversibly stretch over large ranges (i.e., $\gamma_{polyurethane}$ > 500%) with elastic moduli low enough to not affect the local mechanical properties of the textiles.

An extreme use case for textiles that exemplifies the need for mechanically soft and hyperelastic strain gauges is in supersonic parachutes. One of the options comprising them is a rip-stop textile that has thicker threads interwoven in a crosshatch pattern to reinforce against local ruptures.[8,9] As predictive modeling for textiles in complex loading conditions is difficult, there is a need for in situ experimental measurements of the strain state of textile during realistic conditions. Common methods for measuring fabric properties while under load include in situ strain sensors or vision-based tracking systems.[10] Vision-based systems, such as digital image correlation (DIC), do not have to be attached to the specimen and can measure full-field deformation. These methods, however, require a camera, points to track, good lighting, and security of the visual field to ensure the accuracy of the result.[11] These

J. Jo, H. Park
Department of Human Centered Design
Cornell University
Ithaca, NY 14853, USA
A. Xu, A. K. Mishra, H. Bai, R. F. Shepherd
Sibley School of Mechanical and Aerospace Engineering
Cornell University
Ithaca, NY 14853, USA
E-mail: rfs247@cornell.edu
A. Derkevorkian
Jet Propulsion Laboratory
California Institute of Technology
Pasadena, CA 91109, USA
J. Rabinovitch
Stevens Institute of Technology
Hoboken, NJ 07030, USA

The ORCID identification number(s) for the author(s) of this article can be found under https://doi.org/10.1002/admt.202200437.

DOI: 10.1002/admt.202200437

constraints make it difficult to use these methods in active and dynamic situations, such as for the conditions created during NASA/JPL's ASPIRE (Advanced Supersonic Parachute Inflation Research Experiment) project. In these experiments, three high-speed cameras were unable to provide adequate resolution for the canopy strain measurements due to the large length scale involved, and the long distances between the cameras and the parachute surface.[12] During the ASPIRE parachute inflation experiments, ≈15 m diameter canopies inflated in ≈0.5 s with the canopy being located ≈50 m away from the cameras.[12,13] At this ≈50 m s^{-1} expansion rate and low camera magnification, it becomes extremely challenging to collect high resolution/sampling rate images to track the local strains optically.

Hyperelastic elastomer composites with conductive materials like liquid metals,[14,15] carbon nanotubes,[16,17] or graphene[18,19] can cover much larger strain ranges (up to 800%)[18] than previously discussed. These electrical strain sensing systems, however, have issues with hysteresis,[20] non-linear responses,[21] or noise from electromagnetic interference.[6] Additionally, liquid metal is expensive, oxidizes when exposed to air or even when in a soft encapsulation,[22] and stiffens the elastomer around itself.[23,24] Capacitive strain gauges, while showing better linearity than the resistive ones, need to cover relatively large areas than the resistive type to convert the mechanical deformation into the measurable signal at small strains.[25,26]

Fiberoptic sensors have advantages over electronic ones. They are i) immune to the electromagnetic interference that affects electronics, ii) lightweight and occupy small form factors, iii) chemically stable, iv) can encode information in both intensity and wavelength,[27] and v) can sample data at high frequencies (higher than 10 GHz).[28] Their structural properties make them amenable to textile integration techniques: weaving,[29–31] knitting,[32] gluing,[33,34] stitching itself on the textile like a thread,[35,36] and embroidering.[37,38] This manufacturing flexibility has enabled their use in dynamic applications such as wearable electronics[33,39–41] and parachute canopies.[29,35,42]

Fiber Bragg Gratings (FBGs) are commonly used fiber optic strain sensors; however, they require a large, bulky optical interrogation system. Therefore, they are undesirable when integrated with a textile that is designed to be lightweight and portable. The flexible but inextensible, high modulus fibers used with FBGs also run the risk of influencing the local mechanical properties of the textiles they are embedded in and may break during large strains. Stretchable lightguides made of elastomers overcome the brittle and rigid characteristics of conventional optical fibers and enable the large strain sensing ranges required for textile-based technologies, with less effect on the local mechanical properties of the measurand.[38,39,43–47]

In this manuscript, we applied stretchable optical fibers, that we call Optical Lace (OL), as strain gauges for measuring local deformation in high-strength textiles. In particular, we chose to explore textiles used for supersonic parachutes in order to eventually sense extreme deformations during their inflation (**Figure 1**a). The result of our investigation is that OL strain sensors provide accurate (absolute error ≈2.93%; Std. Dev.: 3.02%) strain measurements up to at least the yield strain of textiles we measured, $\gamma_{\text{textile}} = (L - L_0) \cdot L_0^{-1}$ ≈30% where L_0 is textile length after the preload, and L is the instantaneous length of the textile. We applied the OL to measure the deformation of the nylon parachute textiles that are a model material for supersonic parachutes.[8,35,48] We report varying OL shapes and integration schemes and evaluate their resulting gauge factors (i.e., sensitivity to strain). Finally, we also report simulation and mechanical testing results that show our sensor does not appreciably affect the mechanical response of the textile under strain, i.e., it is "mechanically invisible."

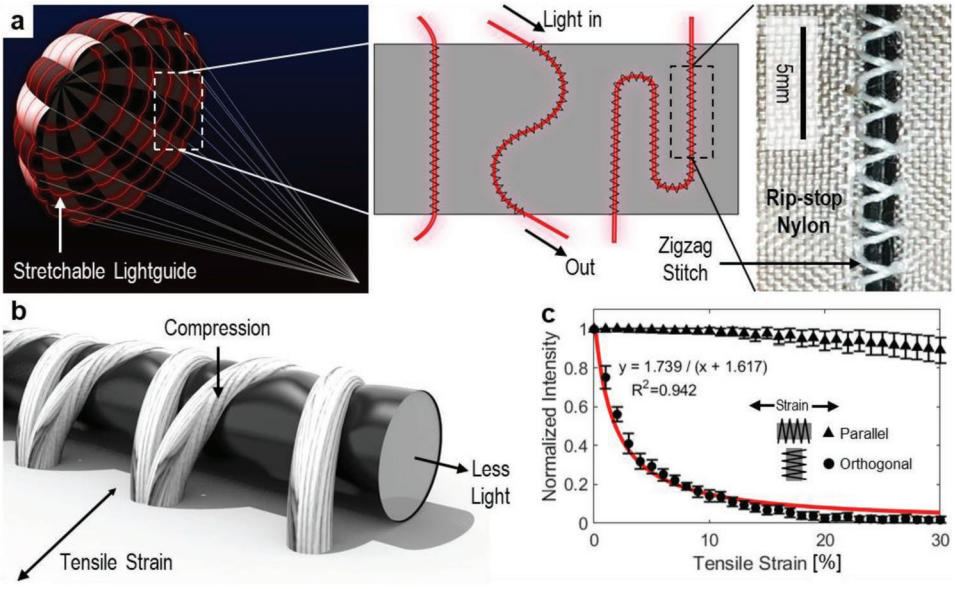

Figure 1. Design overview and sensing principle. a) Potential installation layout on a parachute canopy (left), sensor arrangement examples (center), and OL installed on a rip-stop nylon (right). b) Strain sensing principle. Orthogonal tensile strain on the textile makes the stitch compress the OL, which decreases light transmittance. c) Sensitivity comparison by the direction of the tensile strain of the textile to the OL ($n = 8$).

2. Results and Discussion

2.1. Installation of Stretchable Lightguide on Textile

As a strain gauge, the OL needs to be securely attached to the textile. Weaving and knitting can seamlessly integrate it but limits our choice of optical pathways to achieve the effective performance of the sensor. Threading (e.g., penetrating the textile with the fiber) creates many holes that can potentially degrade the performance of the parachute. Heat sealing (thin polymer tape attached by heat to cover seams) does not securely hold the lightguide. Gluing the fiber is a good option, but it was found that when the modulus of the cladding of a fiber optic is low, small strains of the cladding may not be transferred to the core[49] which lowers sensitivity. The glue also affects the textile's properties and restricts the micro-level movements of the yarns.

Therefore, we used a machine stitch, the most basic, compatible, and repeatable method, to create a mechanical connection between the fiber and textile. It can affect the mechanical properties of the textile but is adjustable by manipulating the stitch density to achieve the original textile properties. In particular, we adopted a zigzag couching stitch (commonly used in embroidery)[39] to hold the OL and textile together without damaging the sensor. In our work, the couching embroidery is not only a medium to attach the sensor to the textile but also the main source of load transfer between the textile and the sensor during tensile strain.

2.2. Directional Sensitivity by Strain Orientation

We found that the orientation of the optical fiber to the strain has a critical impact on the sensitivity. The origin of this directional sensitivity lies in how the stitches interact with the fibers under tension. When tension is orthogonal to the OL, the pressure from the thread and the tensioned textile work similarly to a wire slicer to create indentations on the fiber optic at each stitch-fiber contact site (Figure 1b). The cross-sections of a cladded and a bare fiber optic under 30% strain take on an elliptical shape (Figure S1, Supporting Information); therefore, when light travels inside of the core, the dents make the angle of incidence smaller than critical angle and result in loss of light. The orthogonal sensor was much more sensitive than the parallel one and was able to measure small strains ($\gamma < 1\%$; Figure 1c). The first 1% strain orthogonal to the sensor decreased the light intensity by 24.8% (Gauge factor$_{\perp} = |\Delta I/I| \times \gamma^{1} \approx 24.8$, where I indicates light intensity and γ means the strain) after which the GF gradually decreases as the strain increases. The fastest extension speed of the tensile tester used in this study did not make any difference to the sensitivity and signal trend of OL, nor did the slower loading rate (Figure S2, Supporting Information).

For the OL aligned parallel to the strain direction, on the other hand, the zigzag stitch pulls on the fiber via friction to strain it. Under the assumption that the contact between the fiber optic and the stitching thread is secure enough, the softness of the fiber allows it to be elongated with the textile. This stretching causes attenuation in light intensity due to increased absorption length and shrunk core diameter as described and used in previous research.[39] In this study, however, we observe that the cladding can delaminate from the core, preventing it from stretching properly. Therefore, when tension on the textile is parallel to the fiber, the delamination prevents fiber elongation, resulting in low or no sensitivity to strains in the $\gamma < 30\%$ range before these textiles fail (only 10.7% power output decrease at $\gamma = 0.3$; Std. Dev. = 3.35%) as shown in Figure 1c. Its GF at the first 1% strain was 0.05, in contrast to 24.8 of the orthogonal sensor in the same range.

2.3. Biaxial Sensor with Sinusoidal Arrangement

To explore the potential to detect biaxial tension on the textile, we arranged the fiber optic sensor in a sinusoidal pattern on the textile and stitched it on using the same stitch Figure 1c. Since the sinusoidal curve is longer than a straight line, the number of stitches increased from 12 to 18 per specimen width (25 mm, i.e., 4.8 stitch cm^{-1} to 7.2 stitch cm^{-1}) which creates more dents on the OL. As expected, the sensor arranged in sinusoid reacted to both orthogonal and parallel tension to the textile (**Figure 2**a). While the orthogonal sensor showed rapid light attenuation and lost nearly all of the signal transmitted during the first 5% of strain, the sinusoidal sensor parallel to the tension had a gradual decrease until 20% strain. Both orientations showed higher sensitivity than the straight orthogonal sensor (Figure 1c) which may come from the increased number of the stitches and the sinusoidal arrangement itself.

2.4. Sensitivity Adjustment with Stitch Specification

In the orthogonal strain case, the dents are the main source of sensitivity, so we can adjust it by changing the stitch specification. Frequency indicates how many stitches are in a given length, and amplitude means the width of the zigzag stitch across the fiber optic (Figure 2b). We fabricated four sets of samples with varying frequency and amplitude and compared the signal trends (Figure 2c). First, the frequency is important because each dent causes light loss, with lower frequency resulting in fewer stitches and less sensitivity. Additionally, we find that the power output modulation was more sensitive with stitches with higher amplitude. Stitches create dents on the OL based on the load transferred from the textile, so stitches with higher amplitude will transfer more load to the OL because they cover a larger amount of tensioned textile than the one with lower amplitude. Lastly, the frequency and amplitude affect the angle of the zigzag. If the angle between the thread and the OL is more perpendicular, the strain is more directly translated into denting the fiber. Therefore, a zigzag stitch with high frequency and high amplitude (where the angle is closer to perpendicular than the others) makes the intensity more sensitive to strain. Gauge factor showed differences before 5% strain by the stitch type and then settled down with similarly low level up to the break of the textile (Figure S3, Supporting Information). We further explored other threads and textiles with varying elastic moduli. According to the result, there was no significant relationship between the elastic modulus of threads and

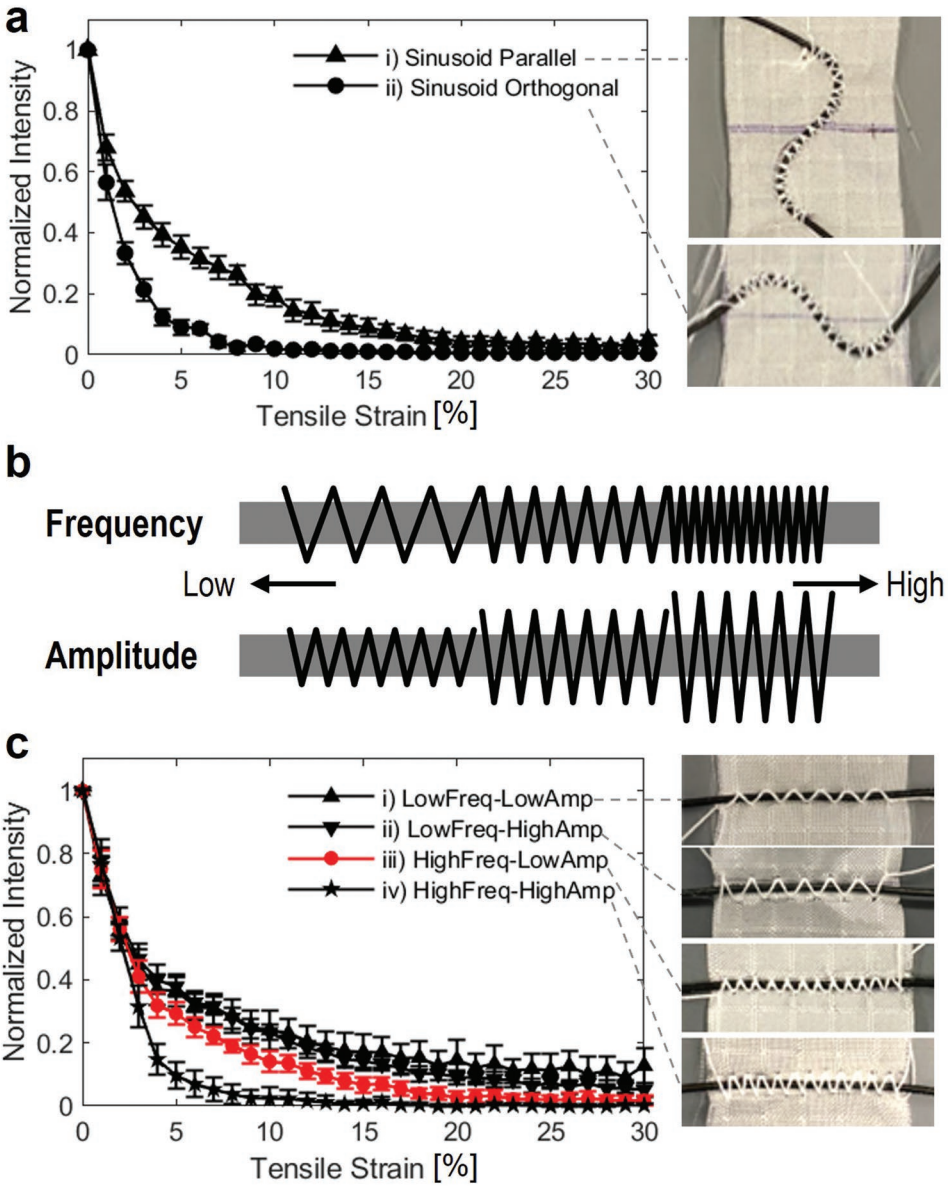

Figure 2. Biaxial sensor and sensitivity by stitch specification. a) Biaxial sensor fabricated as a sinusoid line shape ($n = 5$). b) Schematic showing frequency and amplitude in zigzag stitch. c) Sensitivity to orthogonal strain by frequency and amplitude ($n = 8$). Stitch marked in red is the one that used all the other sensors in this work.

gauge factor at 0–1% strain range, while high-modulus textiles have a tendency to show higher sensitivity at the same range (Figure S4, Supporting Information). Most sewing threads are much stiffer (2.5–11.12 GPa) than the elastomeric lightguide (0.0093 GPa), so the response was not influenced. On the other hand, textiles have a large range of moduli (0.004–0.47 GPa), which does affect the sensitivity of the OL to the strain.

2.5. Mechano-Optical Simulation and Validation

We performed mechano-optical coupled numerical analysis to confirm our hypothesis from the experimental observation—the microbending introduced by stitch compressions is the main reason for high sensitivity in the orthogonally oriented fiber optic. As rays propagate in the deformed fiber, each dent causes light to leak from the fiber, inducing attenuation in the output intensity (**Figure 3**a). This effect was confirmed with simplified experiments done on a Dynamic Mechanical Analysis (DMA) machine (Figure 3b) since simulating textiles is very difficult and the forces applied to the OL by the stitch are non-trivial to derive. With the mechanical simulation setup, we varied the number of struts and, therefore, the stitch frequency. We controlled the total compression force of the whole structure and the indentation force per dent by displacement so the compression was identical in the mechanical simulation and the experiment (Figure S5, Supporting Information). Figure 3c shows as stitch frequency increases, each stitch on

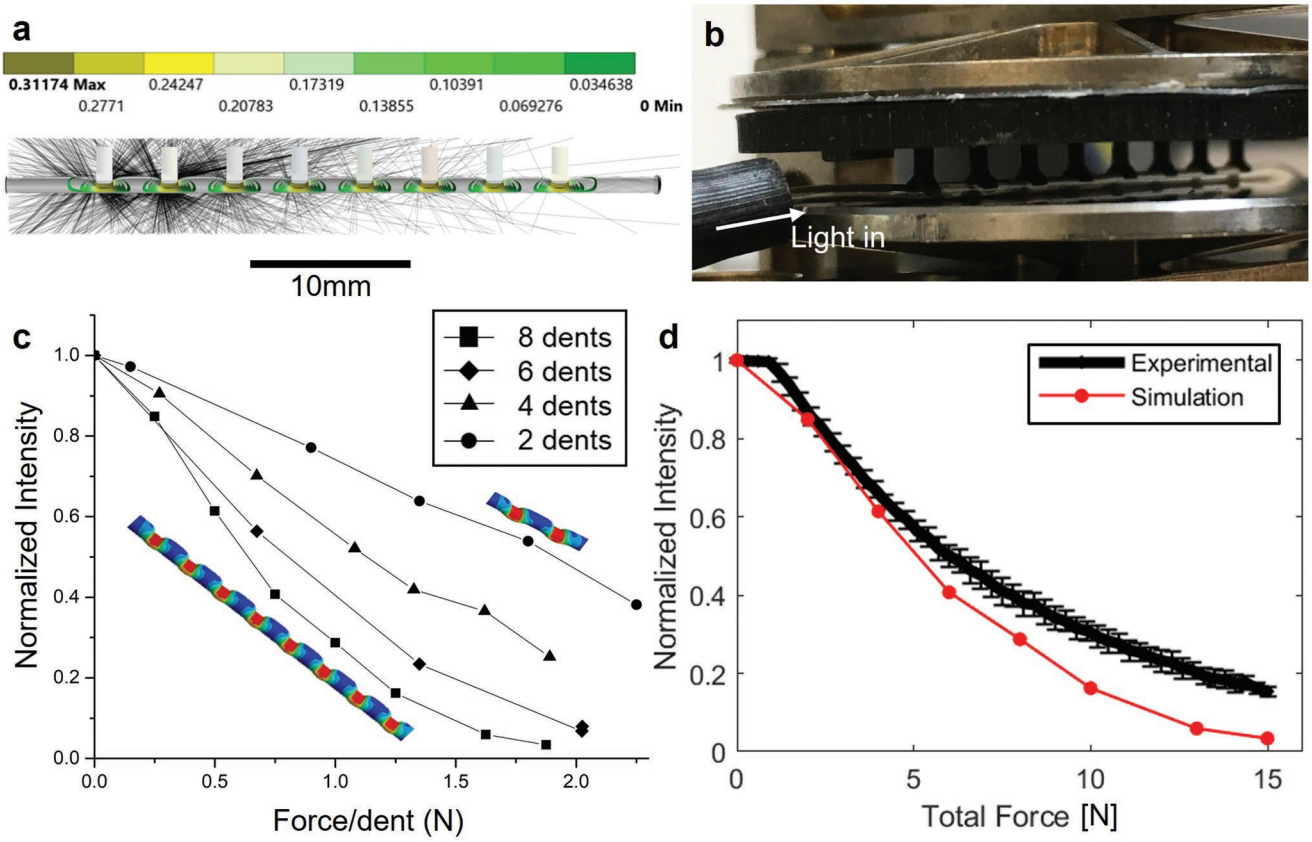

Figure 3. Simulation and experimental validation. a) Mechano-optical simulation of OL with 8 dents. Light leaks around the dents, which results in light attenuation. b) Experimental setting to validate the simulation result. c) Normalized light intensity by indentation force per dent and the number of dents in the optical simulation. d) Comparison of light intensity in ray simulation and experiment ($n = 3$).

average produces less attenuation with the same compression force due to less indentation. Consistent intensity response across different stitch frequencies (Figure S6, Supporting Information). Data from the mechano-optical model shows that the behavior is as expected and is in good agreement with the experimental data (absolute difference≈7.39%; Std. Dev.: 5.70%, Figure 3d). Lastly, the leakage of light at the dents created by the stitch under the tension was also confirmed in a test set with a visible red light (Figure S7, Supporting Information). Wherever the thread on 30% strained textile met the transparent OL was brighter than other parts, which indicates the light leakage at the dents and less light intensity transmitted through the fiber.

2.6. Mechanical Invisibility

We confirm that the OL is mechanically invisible to the nylon fabric by observing the stress–strain curve from our tensile test. We see that the textile with one parallel, one orthogonal, and three orthogonal sensors are each within 1.5 standard deviations of the plain textile response (**Figure 4**a). DIC results comparing the four samples (without fiber, with a parallel fiber, and with a single and three orthogonal ones) showed evenly distributed strain throughout with no visual clue that the implemented fiber optic affects the deformation behavior of the textile specimen (Figure 4b). Additionally, a force-controlled, cyclic tensile test seen in Figure 4c,d showed drift in light intensity as well as in the stress–strain response of the textile. Plastic deformation including pinched yarn arrangement in the woven textile may be the main cause, considering the low hysteresis and drift of the OL shown in the cyclic compression test on the DMA (Figure S8, Supporting Information). Again, the speed of tensile extension did not create significant difference in cyclic test (Figure S9, Supporting Information). This result is especially important to critical, high strain, high-stress applications like supersonic parachutes where differences between the tested material and deployed system could result in total failure of the mission, causing catastrophic losses in time and other resources (e.g., the Mars 2020 mission took ≈8 years for preparation until the actual landing on Mars[50]).

2.7. Multiple Sensors to Measure Local Strain

In the test using 2–4 OLs on one textile specimen, the signal from all the sensors showed a similar trend regardless of the location of the OL (**Figure 5**). This result agrees with the DIC which observed even distribution of local strain throughout the textile. It not only supports the mechanical invisibility described earlier by confirming the number of sensors affects neither the mechanical property of the textile nor the sensitivity

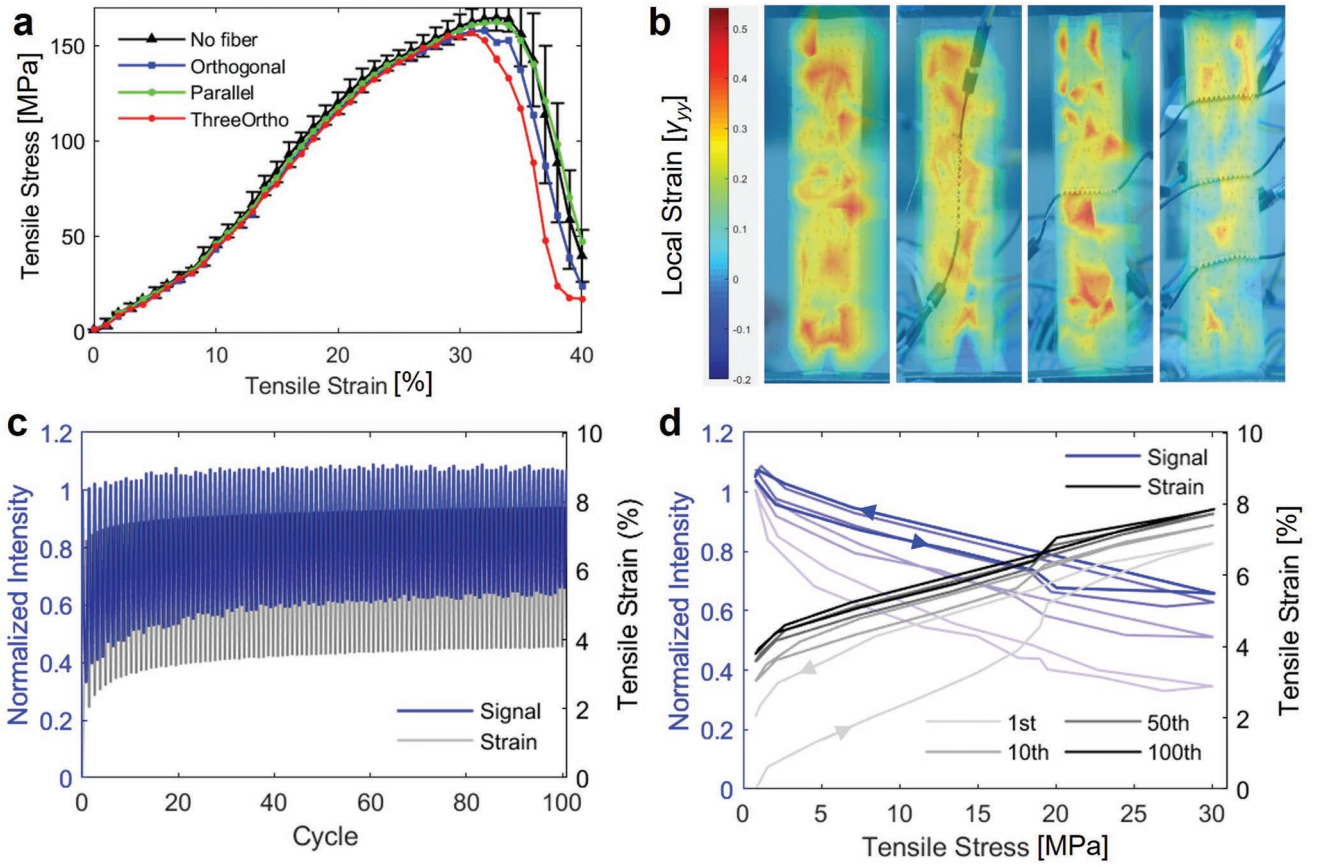

Figure 4. Mechanical invisibility. a) Tensile test results of textiles with varying numbers of OL and direction. Strain–stress curves are identical before breaks of the textile around 30% strain (n>4). b) DIC results showing that OL and the stitch did not result in significantly different strain behavior in the textiles. c,d) Light intensity changes following the drift of strain during the 100 cycles of force-controlled tensile test.

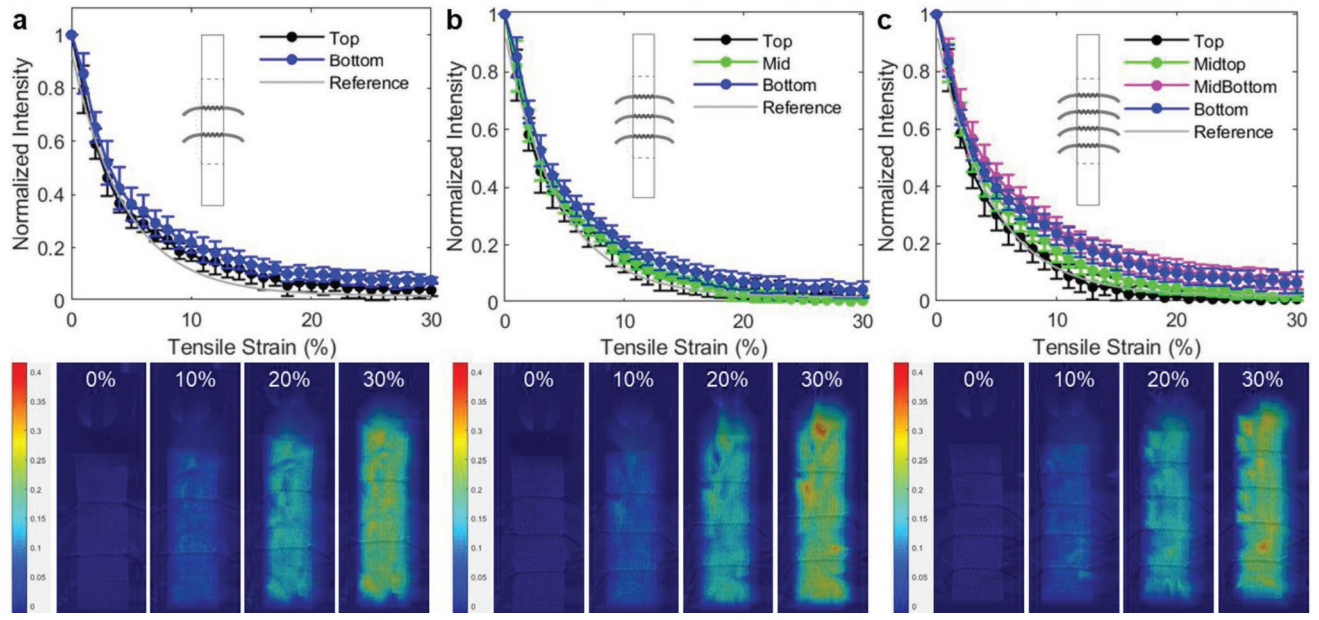

Figure 5. Multiple sensors orthogonal to the strain on the textile. a) Light signal change of two sensors and DIC analysis (n = 4), b,c) Three and four sensors in the same condition respectively (n = 5).

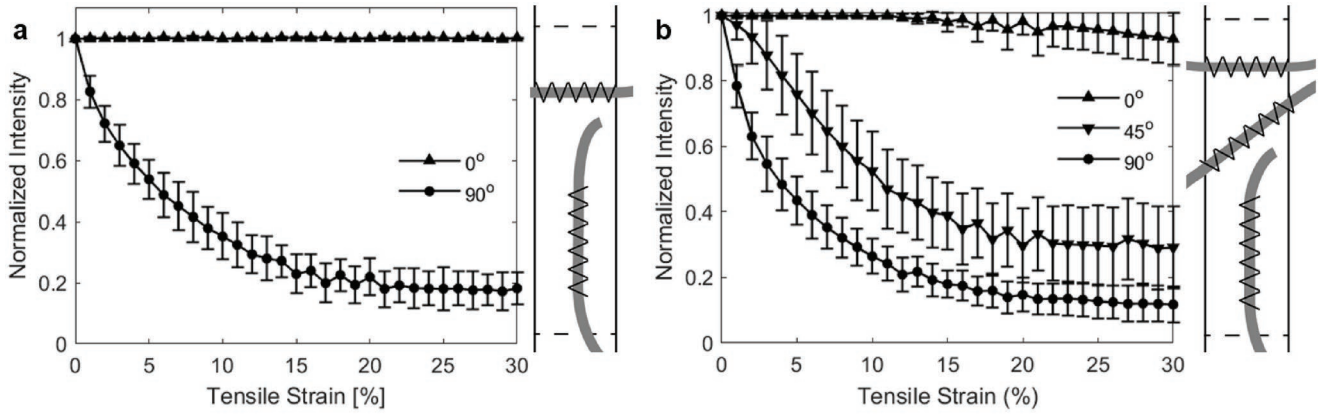

Figure 6. Rosette strain gauges. a) Two sensors in a form of an XY rosette ($n = 3$). b) Three sensors in a form of a rectangular rosette strain gauge ($n = 9$).

of the lightguide sensor but also opens the broad possibility to measure the local strain of a large textile structure with non-uniform load distribution like our application target of parachute canopies.

While the sensor with a sinusoidal pattern reacts to both parallel and orthogonal tension, it is hard to determine the orientation of the load using only one sensor. Still, it is one of the main goals of the strain gauges for parachute testing to understand the amount and direction of local principal strain on the parachute canopy to enhance the structural stability and prevent failure. Based on the directionality of the OL demonstrated in 2.2, we installed multiple fiber optics to create rectangular rosette strain gauge. Two perpendicular sensors (one orthogonal and one parallel to the strain direction, **Figure 6**a) showed that they can differentiate the parallel and orthogonal tension and will be able to define the amount of strain when the direction is known, as an XY rosette strain gauge. Three sensors oriented at 45° to each other in the form of a rectangular rosette also showed identical signal trends with the single sensors in the same direction respectively (Figure 6b; Figure S10, Supporting Information). As a rosette gauge, the grid of sensors will be able to determine the directionality and level of load on the parachute canopy.

3. Conclusion

We applied zigzag stitching onto stretchable fiber optic strain gauges placed on top of nylon parachute textiles for the application of mapping strain during parachute canopy inflation. The threads holding the OL to the fabric press down and create dents on the lightguide under orthogonal tension of the textile, modulating the output signal intensity. The resulting gauge factor is large, ≈24.8 at the first 1% strain making it a sensitive approach to mapping strain in textiles. Coupled mechano-optical simulations confirmed the effect of the local compressions to the fiber by the stitchwork on the light transmittance. We also explored the variations in stitch specification and fiber arrangement; higher amplitude and higher frequencies of the stitch make it more sensitive. Additionally, arranging the fiber in a sinusoidal shape enables biaxial strain sensing. In this study, where we focused on a lightweight, woven parachute textile with high tensile strength, the large and reversible strain of the sensors allowed for accurate strain prediction over large deformations (≈30%). The stitch work transferring the load as compressing dents on the low modulus fiber result in high sensitivity strain gauges that do not affect the mechanics of deformation of the nylon parachute textile.

As demonstrated in this study, our OL sensor can track the strain field of the nylon parachute textile, so we expect it will be able to contribute to understanding the behavior of parachute canopies without adding negative impacts to the performance of the parachute. We confirmed that low-pressure differentials across the canopy textile are measurable by our sensor networks (Figure S11, Supporting Information). Since the direction of the loading on the canopy is still uncertain, installing the OL in two or more directions on the parachute will be beneficial to identify the direction and amount of the tension. It is also promising to take advantage of the OL's cloth compatibility by implementing it on protective garments and sports/outdoor gear to achieve effective motion sensing and other biometric monitoring. Other high tensile strength, textile-based systems such as tents, sails, or safety belt straps can adopt it to track and ensure the stability of a system in real-time. Furthermore, the concept of dents on the fiber optic created by compression of strings or struts can be effective on many systems with soft surfaces other than textiles such as human skin, flexible display panels, and artificial organs.

As supersonic parachutes are never reused, the fatigue that the parachute canopy experiences only come from the packaging process before its first and final inflation during the entry, descent, and landing (EDL) sequence of the spacecraft.[13] As a parachute canopy is folded like an accordion and multiple sensors will be installed to monitor local deformation, some of the sensors may be folded within the packaging. Our folding-unfolding test showed a satisfactory signal recovery after the sensor and textile were unfolded (Figure S12, Supporting Information), but more testing will be required before implementing the OL in an actual parachute test which costs millions of dollars. The temperature range that the sensor will experience during the cruise (≈ –73.15 to 26.85 °C) is slightly out of the coverage of the current fiber (≈ –60 to 160°C) at the lower

boundary.[51] Our sensor demonstrated lesser sensitivity to the tensile load under the temperatures closer to Tg (Figure S13, Supporting Information). There are other elastomer formulations such as fluoroelastomers and Avantor's NuSil that have low Tg and low volatility, compatible with space conditions but their availability is limited with high associated costs. In future work, these materials will hopefully be available for validation in small- and full-scale tests. We also note that extreme deformations (>30%) and cyclic loading over many cycles can peel off the cladding of the fiber optic. To guarantee the durability of the sensor in applications that require repetitive strains such as joints in soft robotics or wearables, the cladding should be able to bear the friction with the thread. Further, microstructures such as seams or stitches could affect the behavior of the fiber optic sensor.

Nevertheless, it has clear advantages for textiles used in inhospitable environmental conditions such as space or magnetic resonance imaging (MRI) facilities, for the fiber optic is lightweight (textile: 6.26 mg cm^{-2}; OL: 9.64 mg cm^{-1}; thread: 0.37 mg cm^{-1}), nonconductive, insensitive to most electromagnetic interference, and chemically inert. Considering the characteristics of textiles, compared to hard materials like metals, the low elastic modulus of the stretchable fibers is beneficial to reduce the effect the sensors have on the mechanical properties of the fabric, which most commercial strain gauges cannot achieve. As a conventional method to attach objects onto a textile, the couching stitch makes the OL production-friendly and can be implemented anywhere stitching is possible.

In future work, multitudes of these sensors can contribute to high-resolution 2D stress–strain mapping over large areas. We can enhance the performance of networks of these fibers by building in directional sensitivity from micro-texturing of the surface[52] or simply employing supervised learning to train and interpret the networks of stretchable fiberoptic sensors for deformation reconstruction. Since these sensors are based on light propagation, it is likely we can collect high-frequency data (>100 kHz) for in situ measurement of supersonic parachutes and use these models for post-experiment analysis of high temporal and spatial resolution canopy inflation dynamics.

Further, while we focused on a very particular application of supersonic parachutes, these sensors also have applications in the space of wearable biometric monitoring, tactile sensing skins for robotics, structural health monitoring, and inflatable fabric structures generally. All of these applications would benefit from textile coats that provide accurate models of kinematics or forceful interactions without affecting the underlying object.

4. Experimental Section

Materials: A rip-stop nylon textile was used for parachute canopies manufactured by Heathcoat Fabrics Limited. This material had an $E \approx 1.57$ GPa, ultimate strain of $\gamma_{ult} \approx 28\%$,[35] and its thickness was 0.11 mm. The textile was woven into broadcloth with a crosshatch pattern with regular intervals that reinforces against ripping and tearing[8] at the peak load experienced by parachutes during supersonic inflation ($\Delta P > 144.56$ kN).[53] To imbue these nylon parachute textiles with strain sensing ability, it was chosen to stitch on the OL composed of a clear, soft, thermoplastic elastomer ($D = 1$ mm, $E_t = 9.3$ MPa, $n = 1.54$; Crystal Tec, Inc.; Figure S14, Supporting Information) core that was clad with silicone ($n = 1.5$, $E_t = 0.4$ MPa; RTV silicone) and then coated with an opaque black silicone ($E_t = 0.4$ MPa, RTV silicone) as depicted in Figure 1b.

Though a wide range of wavelengths can be transmitted well by the fiber,[39] it was chosen to use near-infrared ($\lambda = 875$ nm) light-emitting diodes (TSHA4401; Vishay Semiconductors) to reduce attenuation due to bending and to match the peak sensitivity of the photodiode (SFH-229; Osram Opto Semiconductors). Operational amplifiers (LM324A; Texas Instruments) amplified the light signal with 10-megaohm gains and 4700-pF capacitors. 3D printed connectors aligned the ends of the OL to an infrared LED or photodiode with an Arduino Nano microcontroller reading the analog signal.

Lastly, common industrial, core-spun thread, "Dual Duty" (Coats & Clark Inc., Charlotte, NC), for sewing machines held the fiber optic onto the textile surface. The thread (63% polyester filament core wrapped by 37% mercerized cotton, $D = 0.15$ mm) had to achieve mechanical tenacity, heat resistance, and sewing performance suitable for heavy-duty outdoor use[54] to make the sensor system itself suitable to the supersonic parachute canopy.

Fiber Optic Sensor Fabrication: A strand of the clear, elastomeric fiber was taken and threaded through a blunt tip tapered dispensing fill needle with an opening that is twice the desired coating thickness larger than the diameter of the core. The strand was then hung vertically with the cone tip pointed up for the coating process. The tip was filled, and the core was roughly covered with the clear RTV silicone glue. Then, the tip was carefully pulled down over the fiber to spread out the RTV silicone into a smooth layer. Once that is dry, the process was repeated with the black RTV silicone to create the light-blocking coating.

Uniaxial Tensile Test: To characterize the performance of the strain sensor, 25 mm wide, 0.11 mm thick nylon parachute textile strips were placed with a 60 mm long, zigzag-couched OL between the grips of the tensile testing machine (Instron 5566, Instron, Norwood, MA) with a gauge length of 75 mm according to ASTM D5035-11 (Standard Test Method for Breaking Force and Elongation of Textile Fabrics, Strip Method).[55] The tester pulled each end of the textile at a loading rate of 300 mm min^{-1} after a preload of 0.8 MPa (<0.5% of mean peak stress). 3D printed caps connected each end of the fiber optic to the IR LEDs and photodiodes respectively. The microcontroller sampled the photodiode at 100 Hz (Figure S15, Supporting Information).

The deformation of OL was directly observed under tensile loading of the textile with and without stitched OL using two microscopes: the portable one (USB2-MICRO-200X; Plugable Technologies, Redmond, WA) for the side view, and a tabletop one (Olympus BX51 Microscope) for cross-sectional view. Additionally, a high-speed camera (Phantom MIRO 310) was used to capture the dynamics of the deformations. The tensile test was terminated at $\gamma \approx 30\%$ for observation. While still under tension, the shape of the deformed textile and OL were fixed using glue, and then the sample was laser-cut to reveal the cross-sectional deformation.

For experimental validation, DIC measurements were run during tensile loading. The textile sample was randomly dotted and the video of each test was recorded and each frame was converted into tiff images with MATLAB. Using VIC-2D (Correlation Solutions Inc.), ≈80–140 speckle points were tracked to get the displacement of the dots during the test. Based on the data from the DIC, MATLAB was used to calculate the local strains between points and were plotted as a heat map over the images of the textile.

For tensile tests in varied temperature settings, a dynamic mechanical thermal analysis was conducted using DMA Q800 V7.5 Build 127. The stretchable lightguide on the textile strip was zigzag-stitched in the size of $25 \times 8\,mm^2$ in the center, orthogonally oriented to the tension. When the temperature reached at the target level, the sample stayed for four minutes to be fully soaked. Force ramp rate was 9N min^{-1}, and the upper force limit was 18N on top of the preload of 0.1N at the beginning of tension.

Mechano-Optical Simulation and Validation: Ansys Workbench 19.1 was used for the structural modeling to investigate our hypothesis that

the sensitivity of our strain gauge comes from the dents created on the OL by the tensioned stitches. A 50 mm long stretchable fiber optic indented by eight arc-shaped struts placed 4 mm apart was simulated. The probes were simulated as urethane methacrylate (UMA; elastic modulus, $E \approx 2.1$ GPa, Poisson's ratio 0.35); the stretchable optical fiber core was simulated as thermoplastic polyurethane (TPU; $E \approx 3.0$ MPa, Poisson's ratio 0.48). Finally, the plate (on which the fiber optic is placed) was simulated as structural steel ($E \approx 200$ GPa, Poisson's ratio 0.3). To develop the model, a 3D design from SolidWorks 2018 was first exported and the material properties of the stretchable fiber, base, and struts were defined. Then the body contacts were defined as bonded for both the indentation probe to the fiber and the fiber to the base and Augmented Lagrange formulation was used for the solver. For convergence, minimum penetration was selected. The "Pinball" contact region had a ≈0.1 mm contact radius. The models were meshed using all quad elements with a 0.075 mm element size with 460 548 total number of elements, 1 252 682 total number of nodes, and 148 506 contact elements (Figure S16, Supporting Information). The boundary conditions were then defined, such as the fixed base, and then the compressive force was set as a function of time in 15 steps. To solve the model, an implicit solver was used and solved for the displacement of the indentation. In this case, an Intel (R) Quad Core (TM) i7-6700HQ CPU @ 2.60GHz took ≈9.11 h to solve the fiber indentations for two, four, six, and eight indents individually. More details of the solver can be found in Table S1 (Supporting Information).

To confirm whether the shape of dents caused by tensioned threads and the deformation simulated in the structural modeling was the same, 25 strands of the thread orthogonal were manually sewed to the fiber on the textile and the threads were pulled at 10 mm min^{-1}. The portable microscope was used to observe the side view of the deformed fiber optic. The observed shape of the dents on the OL corresponded with the one created in the simulation (Figure S17, Supporting Information).

Taking the deformation from the mechanical simulation, ray-tracing simulations were then done in COMSOL (Ray Optics) to evaluate the effect on light transmission. Since the optical fibers are 1 mm in diameter, geometric optics can be used to explore the working principle. The deformed fiber placed in the air ($n = 1$) was simulated to have a refractive index of $n = 1.52$ and extinction coefficient of $\Gamma \approx 0.97e^{-6}$ at wavelength $\lambda \approx 875$ nm. A light source was used with Lambertian distribution to simulate the IR LED and collect the intensities at the output of the fiber. These simulations were done for a variety of contact densities (2, 3, 4, and 8 over a 50 mm length).

To validate the simulation model, a compression test was performed using a dynamic mechanical analysis (DMA Q800 V7.5 Build 127) tester on a 50 mm long, 1 mm diameter, bare fiber optic and a 3D printed, rigid polyurethane (RPU) structure to create stitch-like dents. After attaching the 3D printed structure with double-sided tape to the top moving plate, the bare fiber optic was arranged between the bottom plate and the struts. A load of 10 N min^{-1} from 0.01 N to 15 N to compress the fiber with the struts was then applied (Figure 3b).

Wind Test: To examine the sensor behavior to the wind, Frazier Air Permeability Tester was used which generates a low differential air pressure (<24.908 Pa) across the specimen. On the 30×30 cm^2 textile specimen, the 60 mm fiber optic was installed in the center using the standard zigzag stitch. The differential air pressure across the textile gradually increased by 2.4908 Pa and was recorded along with the light intensity.

Statistical Analysis: The light intensity was normalized based on the value at the pre-strained condition. All the data points represent the mean of the samples, and the error bars the 95% confidence interval except ±1.5 SE in Figure 4a. The number of samples for each figure is in the figure caption.

Supporting Information

Supporting Information is available from the Wiley Online Library or from the author.

Acknowledgements

Parts of this research were carried out at the Jet Propulsion Laboratory, California Institute of Technology, under a contract with the National Aeronautics and Space Administration and funded through the Strategic University Research Partnership (SURP) program. This work was also supported in part by National Science Foundation (grant no. EFMA-1830924) and Air Force Office of Scientific Research (grant no. FA9550-20-1-0254). The authors thank Cornell Center for Materials Research Shared Facilities which are supported through the NSF MRSEC program (DMR-1719875) for the use of the facilities.

Conflict of Interest

R. F. Shepherd is a co-founder of a company, Organic Robotics Corporation, that licenses related intellectual properties. The other authors declare no competing interests.

Data Availability Statement

The data that support the findings of this study are available from the corresponding author upon reasonable request.

Keywords

optical sensing, parachutes, textile strain gauges

Received: April 2, 2022
Revised: May 2, 2022
Published online:

[1] J. W. Hearle, W. E. Morton, *Physical Properties of Textile Fibres*, Elsevier, Amsterdam, Netherlands **2008**.
[2] K. Song, Y. Zhang, J. Meng, E. Green, N. Tajaddod, H. Li, M. Minus, *Materials* **2013**, *6*, 2543.
[3] Y. Sun, W. Xu, W. Wei, P. Ma, F. Xia, *J. Ind. Text.* **2019**, *50*, 1384.
[4] C. Mattmann, F. Clemens, G. Tröster, *Sensors* **2008**, *8*, 3719.
[5] "Strain Gage Application Requires Quality Control Surface Preparation and Application Steps," can be found under https://www.omega.com/en-us/resources/strain-gage-quality-control.
[6] M. Amjadi, K.-U. Kyung, I. Park, M. Sitti, *Adv. Funct. Mater.* **2016**, *26*, 1678.
[7] J. A. Fan, W.-H. Yeo, Y. Su, Y. Hattori, W. Lee, S.-Y. Jung, Y. Zhang, Z. Liu, H. Cheng, L. Falgout, M. Bajema, T. Coleman, D. Gregoire, R. J. Larsen, Y. Huang, J. A. Rogers, *Nat. Commun.* **2014**, *5*, 3266.
[8] K. S. Szafran, I. Kramarski, *Fatigue Aircr. Struct.* **2019**, *2019*, 103.
[9] P. A. Annis, *Understanding and Improving the Durability of Textiles*, Woodhead Publishing, Oxford **2012**.
[10] L. D. Peterson, A. Derkevorkian, J. Rabinovitch, C. Farhat, P. Avery, in *2018 AIAA Aerospace Sciences Meeting*, **2018**, p. 1539.
[11] B. Pan, K. Qian, H. Xie, A. Asundi, *Meas. Sci. Technol.* **2009**, *20*, 062001.
[12] J. Rabinovitch, G. S. Griffin, W. Seto, C. O'Farrell, C. L. Tanner, I. G. Clark, *J. Spacecr. Rockets* **2020**, *57*, 1139.
[13] J. R. Cruz, D. W. Way, J. D. Shidner, J. L. Davis, D. S. Adams, D. M. Kipp, *J. Spacecr. Rockets* **2014**, *51*, 1185.
[14] C. B. Cooper, K. Arutselvan, Y. Liu, D. Armstrong, Y. Lin, M. R. Khan, J. Genzer, M. D. Dickey, *Adv. Funct. Mater.* **2017**, *27*, 1605630.
[15] J. Wang, G. Cai, S. Li, D. Gao, J. Xiong, P. S. Lee, *Adv. Mater.* **2018**, *30*, 1706157.

[16] T. Yamada, Y. Hayamizu, Y. Yamamoto, Y. Yomogida, A. Izadi-Najafabadi, D. N. Futaba, K. Hata, *Nat. Nanotechnol.* **2011**, *6*, 296.
[17] D. J. Lipomi, M. Vosgueritchian, B. C. Tee, S. L. Hellstrom, J. A. Lee, C. H. Fox, Z. Bao, *Nat. Nanotechnol.* **2011**, *6*, 788.
[18] C. S. Boland, U. Khan, C. Backes, A. O'Neill, J. McCauley, S. Duane, R. Shanker, Y. Liu, I. Jurewicz, A. B. Dalton, J. N. Coleman, *ACS Nano* **2014**, *8*, 8819.
[19] C. Yan, J. Wang, W. Kang, M. Cui, X. Wang, C. Y. Foo, K. J. Chee, P. S. Lee, *Adv. Mater.* **2014**, *26*, 2022.
[20] Y. Li, Y. A. Samad, T. Taha, G. Cai, S.-Y. Fu, K. Liao, *ACS Sustainable Chem. Eng.* **2016**, *4*, 4288.
[21] I. Kang, M. J. Schulz, J. H. Kim, V. Shanov, D. Shi, *S. Mater. Struct.* **2006**, *15*, 737.
[22] J. Chen, J. Zhang, Z. Luo, J. Zhang, L. Li, Y. Su, X. Gao, Y. Li, W. Tang, C. Cao, Q. Liu, L. Wang, H. Li, *ACS Appl. Mater. Interfaces* **2020**, *12*, 22200.
[23] J. Zhang, M. Liu, G. Pearce, Y. Yu, Z. Sha, Y. Zhou, A. C. Y. Yuen, C. Tao, C. Boyer, F. Huang, M. Islam, C. H. Wang, *Compos. Sci. Technol.* **2021**, *201*, 108497.
[24] M. D. Dickey, *Phys. Today* **2021**, *74*, 30.
[25] T. Dong, Y. Gu, T. Liu, M. Pecht, *Sens. Actuators, A* **2021**, *326*, 112720.
[26] C. Zlebic, N. Ivanisevic, M. Kisic, N. Blaz, A. Menicanin, L.j. Zivanov, M. Damnjanovic, in *2014 29th International Conference on Microelectronics Proceedings – MIEL 2014*, IEEE, Belgrade, Serbia, **2014**, pp. 141–144.
[27] B. Lee, *Opt. Fiber Technol.* **2003**, *9*, 57.
[28] L. R. Chen, M.-I. Comanici, P. Moslemi, J. Hu, P. Kung, *Appl. Sci.* **2019**, *9*, 298.
[29] E. Mendoza, J. Porhaska, S. Mendoza, T. Andreas, Y. Esterkin, J. Bazin, P. Hill, A. Theodosiou, K. Kalli, in *Seventh European Workshop on Optical Fibre Sensors*, (Eds: K. Kalli, S. O. O'Keeffe, G. Brambilla), SPIE, Limassol, Cyprus **2019**, pp. 391–398.
[30] J. Schuster, M. Trahan, D. Heider, W. Li, *Composites, Part A* **2003**, *34*, 855.
[31] J. Wang, B. Huang, B. Yang, *Text. Res. J.* **2013**, *83*, 1170.
[32] A. Chen, J. Tan, P. Henry, X. Tao, *J. Text. Inst.* **2020**, *111*, 745.
[33] M. Ciocchetti, C. Massaroni, P. Saccomandi, M. A. Caponero, A. Polimadei, D. Formica, E. Schena, *Biosensors* **2015**, *5*, 602.
[34] L. Presti, C. Massaroni, P. Saccomandi, M. A. Caponero, D. Formica, E. Schena, in *Conference Proceedings: IEEE Engineering in Medicine and Biology Society. Annual Conference*, **2017**, pp. 4423–4426.
[35] M. El-Sherif, K. Fidanboylu, D. El-Sherif, R. Gafsi, J. Yuan, K. Richards, C. Lee, *J. Intell. Mater. Syst. Struct.* **2000**, *11*, 407.
[36] M. Li, Y. Li, in *Advanced Sensor Systems and Applications II*, International Society For Optics And Photonics, Beijing, China **2005**, pp. 104.
[37] B. Selm, M. Rothmaier, M. Camenzind, T. N. Khan, H. Walt, *J. Biomed. Opt.* **2007**, *12*, 034024.
[38] B. Selm, E. A. Gürel, M. Rothmaier, R. M. Rossi, L. J. Scherer, *J. Intell. Mater. Syst. Struct.* **2010**, *21*, 1061.
[39] C. K. Harnett, H. Zhao, R. F. Shepherd, *Adv. Mater. Technol.* **2017**, *2*, 1700087.
[40] B. Najafi, H. Mohseni, G. S. Grewal, T. K. Talal, R. A. Menzies, D. G. Armstrong, *J. Diabetes Sci. Technol.* **2017**, *11*, 668.
[41] Z. Gong, Z. Xiang, X. OuYang, J. Zhang, N. Lau, J. Zhou, C. C. Chan, *Materials* **2019**, *12*, 3311.
[42] J. M. Bazin, E. Mendoza, B. A. Tutt, P. Hill, in *AIAA Aviation 2019 Forum*, **2019**, p. 2891.
[43] A. Leal-Junior, L. Avellar, A. Frizera, C. Marques, *Sci. Rep.* **2020**, *10*, 13867.
[44] H. Bai, S. Li, J. Barreiros, Y. Tu, C. R. Pollock, R. F. Shepherd, *Science* **2020**, *370*, 848.
[45] P. A. Xu, A. K. Mishra, H. Bai, C. A. Aubin, L. Zullo, R. F. Shepherd, *Sci. Rob.* **2019**, *4*, eaaw6304.
[46] H. Bai, S. Li, R. F. Shepherd, *Adv. Funct. Mater.* **2021**, *31*, 2009364.
[47] H. Zhao, K. O'Brien, S. Li, R. F. Shepherd, *Sci. Rob.* **2016**, *1*, eaai7529.
[48] C. Cochrane, M. Lewandowski, V. Koncar, *Sensors* **2010**, *10*, 8291.
[49] D. C. Betz, L. Staudigel, M. N. Trutzel, M. Kehlenbach, *Struct. Health Monit.* **2003**, *2*, 145.
[50] M. Wall, "NASA to Launch New Mars Rover in 2020," can be found under https://www.space.com/18763-nasa-new-mars-rover-2020.html, **2012**.
[51] C. D. Karlgaard, J. Tynis, C. O'Farrell, B. Sonneveldt, in *AIAA Scitech 2019 Forum*, American Institute Of Aeronautics And Astronautics, San Diego, California, **2019**.
[52] H. Zhao, J. Jalving, R. Huang, R. Knepper, A. Ruina, R. Shepherd, *IEEE Robot. Autom. Mag.* **2016**, *23*, 55.
[53] C. O'Farrell, C. Karlgaard, J. A. Tynis, I. G. Clark, in *2018 IEEE Aerospace Conference*, IEEE, Big Sky, MT, USA **2018**, pp. 1–18.
[54] "Dual Duty | Polyester Cotton Corespun Thread | Coats Industrial – Coats," can be found under https://coats.com/en/Products/Threads-and-Yarns/Dual-Duty/Dual-Duty.
[55] ASTM D5035-11, *Standard Test Method for Breaking Force and Elongation of Textile Fabrics (Strip Method)*, ASTM International, West Conshohocken, PA, **2015**.